A study of the valence photoelectron spectrum of uracil and mixed water-uracil clusters

Giuseppe Mattioli, Lorenzo Avaldi, Paola Bolognesi, Annarita Casavola, Filippo Morini, Thomas van Caekenberghe, John Bozek, Mattea Castrovilli, Jacopo Chiarinelli, Alicja Domaracka, et al.

A study of the valence photoelectron spectrum of uracil and mixed water-uracil clusters.

Giuseppe Mattioli[1], Lorenzo Avaldi[1*], Paola Bolognesi[1], Annarita Casavola[1], Filippo Morini[2], Thomas Van Caekenberghe[2], John D. Bozek[3], Mattea C. Castrovilli[1], Jacopo Chiarinelli[1], Alicja Domaracka[4], Suvasthika Indrajith[4], Sylvain Maclot[5], Aleksandar R. Milosavljević[3], Chiara Nicolafrancesco[3,4], Christophe Nicolas[3] and Patrick Rousseau[4]

[1]CNR-Istituto di Struttura della Materia, Area della Ricerca di Roma 1, CP 10, Monterotondo Scalo, Italy.
[2] X-lab, Faculty of Sciences, University of Hasselt, Campus Diepenbeek, BE 3590 Diepenbeek, Belgium
[3]Synchrotron SOLEIL, L'Orme de Merisiers, 91192, Saint Aubin, BP48, 1192, Gif-sur-Yvette Cedex, France.
[4]Normandie Univ, ENSICAEN, UNICAEN, CEA, CNRS, CIMAP, 14000 Caen, France.
[5] Institut Lumière Matière, UMR5306 CNRS, Université Claude Bernard Lyon 1, 69622 Villeurbanne CEDEX, France

*Corresponding author : lorenzo.avaldi@ism.cnr.it

Abstract

The valence ionization of uracil and mixed water-uracil clusters has been studied experimentally and by *ab initio* calculations. In both measurements the spectrum onset shows a red shift with respect to uracil molecule, with the mixed cluster characterized by peculiar features unexplained by the sum of independent contributions of the water or uracil aggregation. To interpret and assign all the contributions, we performed a series of multi-level calculations, starting from an exploration of several cluster structures using automated conformer-search algorithms based on a tight-binding approach. Ionization energies have been assessed on smaller clusters via a comparison between accurate wavefunction-based approaches and cost-effective DFT-based simulations, the latter applied to clusters up to twelve uracil and thirty-six water molecules. The results confirm that *i)* the bottom-up approach based on a multilevel method (Mattioli et al. PCCP 23, 2021, 1859) to the structure of neutral clusters of unknown experimental composition converges to precise structure-property relationships and *ii)* the coexistence of pure and mixed clusters in the water-uracil samples. A natural bond orbital (NBO) analysis performed on a subset of clusters highlighted the special role of H-bonds in the formation of the aggregates. The NBO analysis yields a second-order perturbative energy between H-bond donor and acceptor orbitals correlated with the calculated ionization energies. This sheds light on the role of the oxygen lone-pairs of the uracil CO group in the formation of strong H-bonds, with a stronger directionality in mixed clusters, giving quantitative explanation for the formation of core-shell structures.

1. Introduction

The measurements of the photoelectron spectrum and photoelectron angular distribution of the outer-valence shell of molecules in the gas phase using tunable synchrotron radiation provide invaluable information on the electronic structure and its variations depending on structural changes, that affect the stability and reactivity of the molecule. A broad literature exists on photoelectron spectra of organic molecules of biological interest: from

the building blocks of molecules of life, like DNA bases and their derivatives, to peptides and antibiotic[1].

Of paramount importance is how these molecules interact among each other as well as with water, the solvent of choice for these molecules to perform their bio-functions. H-bonds and π-stacking interactions as well as van der Waals forces define the structural arrangement, i. e. the tertiary and quaternary structure of the large biomolecules. These same interactions play also a key role in molecular recognition processes, like protein-protein or protein-ligand interactions. Such an information cannot be achieved by the study of isolated molecules, and is elusive in bulk solution studies where molecules are highly dispersed, but can be approached by the investigation of molecular clusters of increasing size in the gas phase. These clusters represent the prototypes of weakly bound systems[2] hold together by non-covalent interactions not perturbed by external agents, which may modify the distribution of their electronic charge or disrupt the networks of weak interactions as in the solvation process. Typical methods of production of cluster beams generate a distribution of sizes. This fact limits the experimental descriptions of weak non-covalent interactions in complex aggregates. Such an experimental limit can be overcome by close comparison between experiments and atomistic simulations, which can describe structures and properties of large aggregates at a precision unattainable by experiments. A combined theoretical and experimental investigation of biomolecular clusters has a twofold value. While on one hand the measurements on unselected clusters strictly require theoretical interpretation, on the other one they can validate the structures and interaction identified by theoretical simulations provided a close match between experiments and simulations exists.

While some attention has been paid since the previous century to the characterization of the valence ionization and the size dependent vertical ionization energy of water clusters produced with different approaches, like for example gas discharges[3] and seeded[4]/not seeded[5，6] supersonic beams, less work exists for other molecular clusters. Nucleobase clusters in interaction with multiply charged ions[7-91011] have been investigated with the main goal to associate their fragmentation to the radiation damage. As for the study of the effect of the water environment in which biomolecules are embedded and perform their functions, hydrated clusters with one or few organic molecules have been studied by

multiphoton ionization[12,13], electron impact[14,15] and multiply charged ion impact[8,9]. To our best knowledge no valence photoelectron spectra have been previously reported.

In this context we have undertaken an overall investigation of the valence and core regions of uracil and mixed water-uracil clusters produced in a gas aggregation source by photoelectron spectroscopy at synchrotron SOLEIL. In two previous works[16,17] we have presented the XPS spectra of uracil and mixed water-uracil clusters in the gas phase and highlighted the key role of H-bonds in the organization of supramolecular aggregates. In the case of the homogeneous clusters[16] it was found that the formation of large clusters (up to 50 uracil molecules) is driven by the anisotropic distribution of H-bond donor and acceptor sites, which can be also modulated by weaker dispersion forces, particularly involving π-conjugate charge distributions. In the mixed clusters[17] the presence of hydrophobic moieties leads to the formation of a core-shell-like supramolecular organization in clusters of increasing size, where water forms tightly packed cores and uracil forms a shell around these cores. This peculiar phase resembled neither the uniform mixing typical of hydrated crystals, nor the sharp separation due to solvation. Here we present a combined experimental and theoretical study of valence shell photoionization of both uracil and water-uracil clusters. Measurements have been performed using synchrotron radiation at 80 eV with the goal of confirming the structure-properties relationships observed in our previous contributions[16,17] and to validate the theoretical approach proposed in [16,17] via the direct quantitative comparison with high level theoretical methods. The cluster spectra are interpreted via the calculation of the ionization energies of the different bands using a bottom-up approach, i. e. through clusters of increasing size, using the optimized structures from our recent work[17].The outer-valence Green's function (OVGF) method[18,19], has been adopted to evaluate the ionization energies for aggregates with up to six uracil molecules or four uracil and twelve water molecules for pure or mixed clusters, respectively. A further approach to simulate clusters of larger sizes, up to twelve uracil and thirty-six water molecules, based on Density Functional Theory (DFT) has been also pursued. There is no formal justification in the use of Kohn-Sham eigenvalues as estimates of ionization energies. Nevertheless, such an approach can be justified *a posteriori* by the close similarity often obtained between DFT energies and photo-emission measurements as well as by comparison with accurate albeit much more expensive calculations, which cannot be applied to more than a few molecules[20]. In such

large systems, DFT represents not only an optimal trade-off between accuracy and computational cost, but also the only way to estimate the composition of large molecular aggregates. In the present case, the use of DFT has been validated by a comparison of its results, up to six-molecule aggregates, with accurate calculations made with the Equation of Motion (EOM) Coupled Cluster Single and Double excitations method (CCSD)[21].

Details of the experimental procedure and set-up are reported in section 2 of the paper, while section 3 is devoted to a description of the theoretical approaches used to predict the photoelectron spectrum and to analyze the chemical and physical properties of the studied clusters. The results are collected in section 4, while their discussion based on the theoretical simulations of the spectra and an analysis of the chemical-physics properties of the aggregates, like the stabilization energy, its relationship with the ionization energy and bond orders, are reported in section 5. Section 6 finally is devoted to a summary and some conclusions.

2. Experimental

The experiments have been performed at the PLEIADES beamline of the synchrotron radiation facility SOLEIL, where a cluster source has been mounted in the dedicated Multi-Purpose Source Chamber (MPSC)[22]. To produce a beam of neutral molecular clusters in the gas phase a newly designed gas aggregation cluster source was used[23]. The operation and performances of the source, designed according a source used in the CIMAP laboratory (Caen, France) have been described in [23] and will not be repeated here. The molecular uracil vapor is produced by evaporation of a commercial powder (Sigma Aldrich; purity 99%) in a resistively heated oven at a temperature of about 175°C placed inside the source. In order to produce hydrated species, the He buffer gas flows inside a Nafion tube immersed in ultrapure water[14,15,23]. The valence photoelectron spectra were recorded at photon energies of about 80 eV and the monochromator slit was set to 400 µm. The ejected photoelectrons have been detected by a Scienta R4000 electron energy analyzer equipped with a wide-angle entrance lens (±30° aperture). In the present experiment, the analyzer has been operated at a pass energy of 100 eV, with 600 µm slits (energy resolution about 200 meV). In the range of the kinetic energies of the photoelectrons measured in the

present experiment the transmission of the analyzer varies of about 10%, thus the measured spectra have not been corrected for the transmission of the analyzer. The He 1s peak of the buffer gas used in the gas aggregation source has also been used to calibrate the scale of the kinetic energy of the photoelectrons.

The option to vary the direction of the linear polarization of the incident radiation depending on the settings of the permanent magnets of the APPLE II undulator has been exploited to determine the asymmetry parameter β. In the dipole approximation for randomly oriented molecules and the detection of the electrons in a plane perpendicular to the photon direction of propagation the photoionization differential cross section is given by

$$d\sigma/d\Omega \propto [1 + \beta/4\,(3cos2\vartheta + 1)]$$

if the incident radiation is fully polarized. ϑ is the angle between the direction of the photoelectrons and the polarization direction of the radiation. By rotating the polarization direction of the radiation, while keeping the electron analyzer fixed, two valence spectra have been measured and the β value has been extracted.

The photoemission spectrum of the uracil molecule, used as a reference for the cluster spectra along the paper, has been measured by Feyer *et al.* [24] at the Gas Phase Photoemission beamline of Elettra at 99 eV photon energy using the VG-220i hemispherical electron energy analyzer[25].

3. Theory

In order to calculate the valence spectrum, a bottom-up procedure beginning with the isolated molecule and then moving to clusters of increasing size, has been adopted. The full geometry optimization procedure to find the ground state geometrical parameters has been described previously[17] and only a brief summary will be repeated here. A preliminary and wide screening of homogeneous water and uracil, as well as mixed hydrated uracil clusters has been performed by using a semiempirical tight-binding method rooted in the GFN2-xTB Hamiltonian, as implemented in the xTB suite of programs[26,27]. We have tested the results in smaller, albeit representative, systems such as the mixed clusters of 2 uracil and n water molecules illustrated in Mattioli et al.[17] against *ab-initio* simulations, finding energy landscapes in full agreement with tight-binding results. It should be noted that the adopted procedure[28] cannot guarantee that the converged minimum is the actual global

minimum in the largest investigated systems containing several hundreds of atoms in non-covalently bonded molecules. However, the procedure is sound, so that we can consider converged structures as educated guesses, quite close or energetically almost equivalent to the global minimum. DFT simulations of the valence photoionization spectrum at the dispersion-corrected B3LYP-D3 level of theory have been performed in a plane-wave/pseudopotential framework by using the Quantum Espresso suite of programs[29,30]. As introduced above, in order to provide a comparison, we also calculated ionization energies of uracil aggregates up to the hexamer using the Equation of Motion (EOM) Coupled Cluster Single and Double excitations method (CCSD)[21] as implemented in the ORCA suite of programs[31].

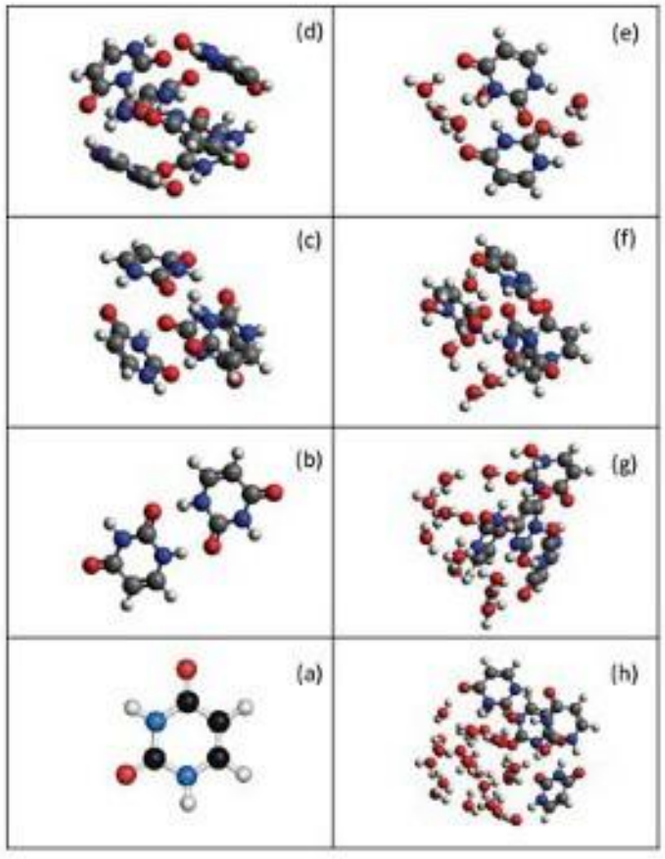

Figure 1: The most stable structures of clusters of 1,2,4 and 6 uracil molecules (a-d), and of mixed water-uracil cluster [(e) 2 uracil molecules and 6 water molecules and (f-h) 4 uracil molecules and 6, 12 and 24 water molecules]. See text.

The good quality of the B3LYP description is confirmed by the reasonable agreement with the more refined calculations using the CCSD approach, once the eigenvalues are corrected

by a rigid shift of 2.3 eV, as shown in the Supplementary Information S1, while the robustness of the DFT-based method has been tested using two other exchange-correlation DFT functionals, namely PBE and PBE0, and proved by the comparison of the simulated spectra with the measurements, as discussed in detail in the Supplementary Information S8.

For a reduced subset of structures (Figure 1) the theoretical ionization spectra have also been calculated using the OVGF method[18,19] in conjunction with the Pople's 6-31G basis set [32] within the GAUSSIAN 09 package [33] . Despite OVGF being a highly cost-effective approach in comparison to others, such as ADC(3)[34- 36]and SAC-CI[37,38], in the calculation of orbital energies, it is not possible to apply it to larger clusters yet. This is due to the scaling which goes as OV^4 (where O and V are the number of occupied and virtual molecular orbitals (MOs), respectively). Another shortcoming is the range of application of OVGF, that is usually limited up to ~ 20 eV and to the pole strength for which this treatment holds ~ 0.85. Below this value the orbital picture of ionization breakdown and shake-up states appear, which account for further correlation[39]. This is certainly the case for systems such as these clusters with π electrons, which may give origin to shake-up states already in the outer valence region. Still, OVGF has proven itself as a solid methodology to study photoionization processes[18,19].

In order to check the effect of the size of the basis set in the representation of the valence ionization spectrum, OVGF simulations have been performed on a uracil dimer using Dunning's correlation-consistent basis set[40] of increasing quality. The results are presented and discussed in Supplementary Information S2 where they are also compared with a similar extrapolation performed within the EOM-CCSD approach using Ahlrics basis sets[41,42].

Natural Bond Orbital (NBO) analysis[43,44] provides an effective and widely used approach for estimating H-bonding energies of individual H-bonds[45,46]. The NBO calculations have been performed on the same subset of structures (Figure 1b-g) using HF/6-31G level of theory. These calculations have been performed using the NBO 3.1 package [47] available in GAUSSIAN 09[33]. The second-order perturbative energy, E(2), between the different Lewis-type donor (filled) and non-Lewis-type acceptor (empty) orbitals has been calculated. The results of these calculations provide an estimation of the delocalized interaction among the different units that compose the clusters in terms of the occupancy from the localized NBOs

of the ideal Lewis structure into the empty non-Lewis orbitals, thereby showing a mismatch from the idealized Lewis structure description. The resulting $E(2)$associated with such a delocalization for a donor NBO (i) and acceptor NBO (j) is defined as

$$E(2) = \Delta(E_{ij}) = q_i \frac{F(i,j)^2}{\varepsilon_j - \varepsilon_i},$$

where q_i is the donor orbital occupancy, ε_i, and ε_j are the orbital energies, and $F(i,j)$ is the off-diagonal NBO Fock matrix element. The outcome of such calculations includes insight into the role of the stabilization energy of the clusters due to the different types of hydrogen bonds and the electronic properties involved in solvation or hydration of uracil. In the selection of the relevant hydrogen bond interactions for the NBO analysis a cut-off of $E(2) > 5$ kcal mol^{-1} was used based on estimates from previous studies[48].

4. Results

Valence photoelectron spectra in the binding energy region 8-22 eV of the uracil molecule (bottom panel), uracil clusters (central panel) and mixed water-uracil clusters (top panel) are shown in Figure 2. Several studies of the photoelectron spectrum of the uracil molecule have been reported in literature[49-58].

	Uracil molecule - ionization potential (eV)				
	OVGF	*ADC(3)*	*DFT*	*EOM-CCSD*	*Experiment*
	9.26[a]	*9.24 [b]*			*9.46 (±0.02) [a]* *9.56 [c]* *9.3(±0.05) [e]*
This work	*9.01[d]*	*9.06[d]*	*7.15*	*9.7*	

*(a)Ref. [57] 6-311++G** basis set; (b) Ref. [57] 6-311G* basis set; (c) Ref. [24] (d) cc-pVDZ basis set;(e) Ref. [58]*

Table 1: Comparison of the theoretical ionization potential of the uracil molecule and the position of the first feature in the experimental photoelectron spectrum.

According to the high-resolution photoelectron spectrum of Fulfer et al.[58] the four outer valence electronic states appear at 9.3, 9.9, 10.5 and 10.95 eV, respectively. The position of the first valence state in the different experimental measurements is compared with the calculations of the ionization potential in Table 1. A general good agreement between

theoretical predictions and experimental value exists, but for the DFT which underestimates the experimental IP by more than 2 eV. Once this rigid shift is applied to the energy levels calculated by DFT a good agreement with the experiments is achieved (see Figure 1. SI in Supplementary Information).

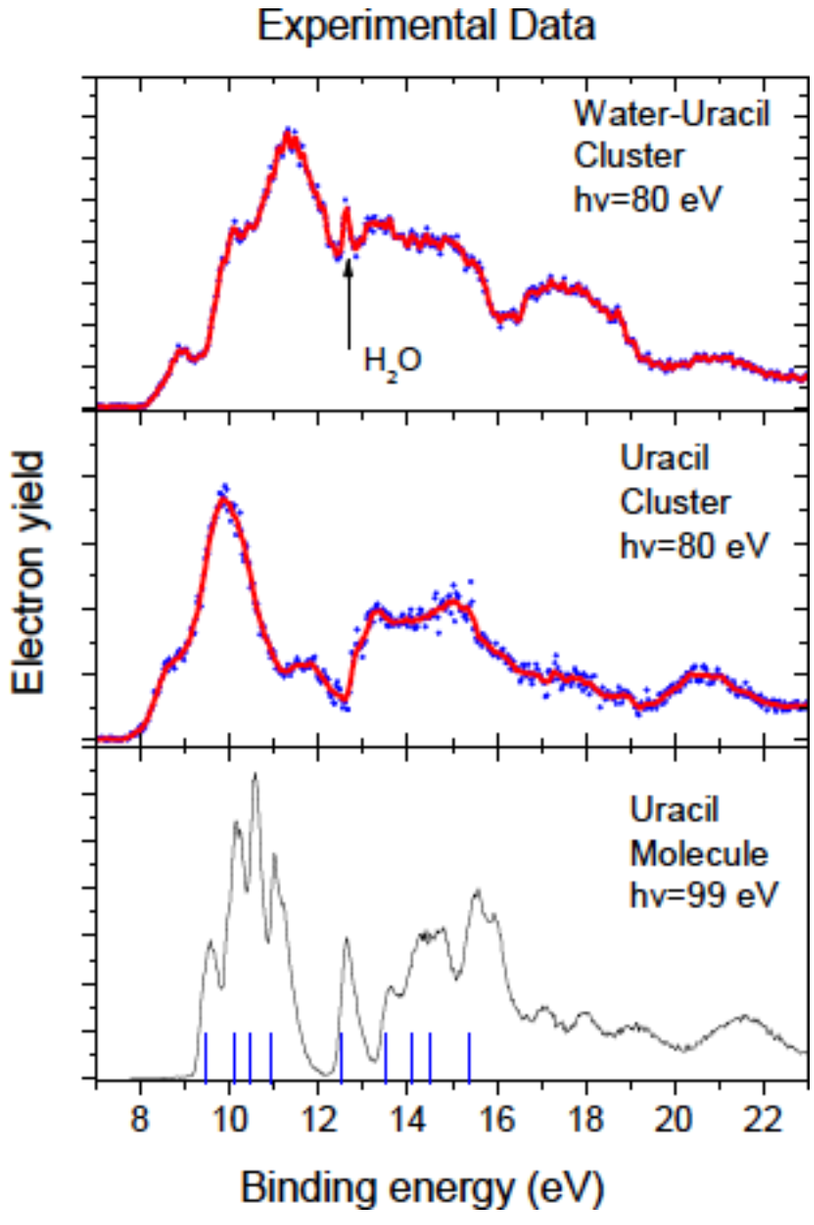

Figure 2: The experimental photoemission spectra of uracil molecule (bottom panel) measured by V. Feyer et al. [24] at 99 eV, of uracil clusters (central panel) and water-uracil clusters (top panel) measured in this work at 80 eV. The bars in the bottom panel represent the maxima of the photoelectron band in ref. [57]. The blue dots in the top and central panels are the experimental values and the red full lines their smoothing.

In the uracil clusters (Figure 2 central panel) the whole spectrum is broadened and the ionization energy is red shifted by about 0.8 eV. Specific features observed in the molecular

spectrum have disappeared, but the general shape of the spectrum is not altered. In the first feature which extends between 8 and 12 eV a shoulder at about 8.8 eV, a central peak at 9.9 eV and then another structure at about 11.7 eV are observed. A broad feature (13-16 eV) encompasses the region where in the monomer the bands assigned to the orbitals between the 2a''(π_3) and 12 a'(σ) were located. The decreasing tail of this feature includes the contributions of the broad bands observed in the monomer between 16 and 20 eV. Finally, a further band is clearly distinguished at about 21 eV.

In the case of the mixed water-uracil spectrum (Figure 2 top panel) the overall shape is quite different from that of the monomer and pure uracil clusters. Beside a tiny blue shift of the ionization potential with respect to the spectrum of the uracil clusters, now the dominant feature appears just above 11 eV, and it is accompanied by the sharp peak assigned to the 1^2B_1 state of isolated water molecules. As also suggested by previous XPS measurements[17], we can expect several contributions to this spectrum: uncondensed water molecules, clearly identified by the sharp peak at 12.62 eV[59], pure water and uracil clusters, and mixed water-uracil clusters.

The contribution of pure water clusters to the spectrum of the mixed clusters can be identified comparing the present data and the photoelectron spectra of water clusters produced by a supersonic expansion in ref. [6] and the one of water molecules shown in the bottom panel of Figure 3. The 1^2B_1 state of water with its typical vibrational distribution is centered at 12.62 eV (ν=0) eV, while the contribution of the water clusters is represented by a broad feature whose centroid shifts towards 11 eV depending on the cluster size. In the top panel of the same figure the measured photoelectron spectra of the mixed and uracil clusters in the binding energy region below 14 eV are shown, while in the central panel the difference of the two spectra is reported. The difference has been obtained after a normalization of the areas of both spectra over the binding energy region 8-23 eV to the same value. This figure indicates that the feature peaking at about 11.5 eV is due to “water clusters” with a size of a few tens of molecules.

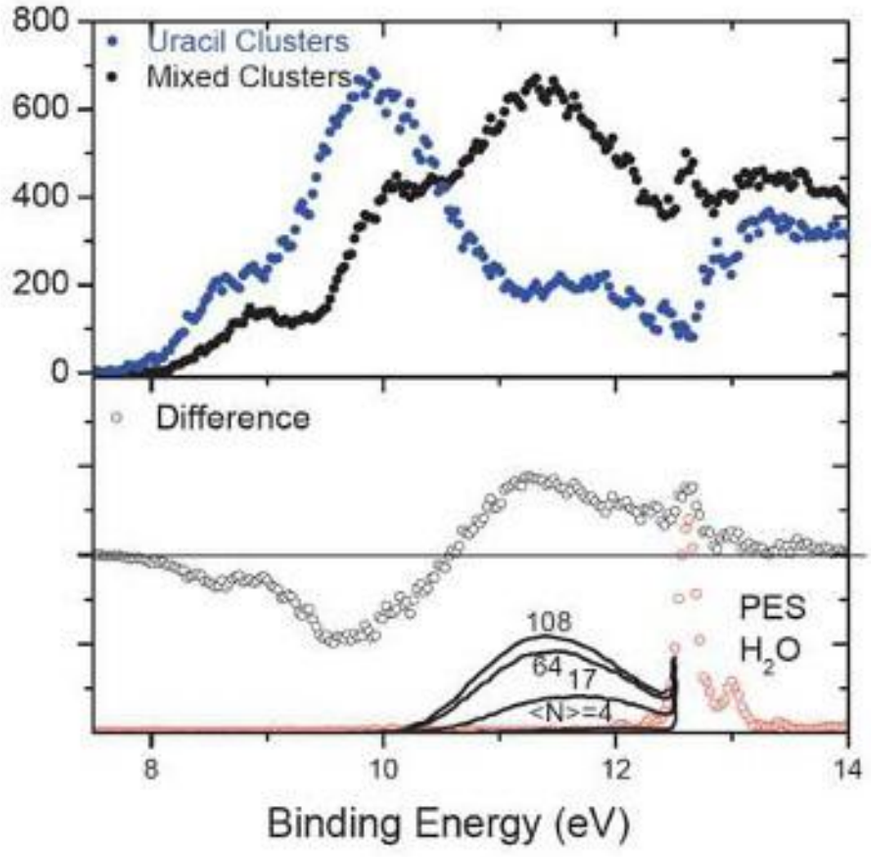

Figure 3: (top panel) The photoelectron spectra of the mixed (black dots) and uracil (blue dots) clusters. (middle panel) The difference between the photoelectron spectra of mixed and uracil clusters of the present experiments (bottom panel). The photoelectron spectra of water molecules (red open circles) and water clusters full lines) digitized from ref. [6].

The asymmetry parameters β of the uracil clusters are reported in Figure 4, where they are compared with those of the uracil molecule measured at 40 eV[57]. In the case of the molecule the difference in the β values, with those associated to π-orbitals higher than those of σ-orbitals[60,61], has been used to complete the assignment of the different bands. In the clusters a decreasing trend from $\beta \approx 1$ at the ionization potential to 0.75 at BE of 23 eV is observed. At 8.87 and 11.87 eV a rise to β=1.1 and 1.25 can be noted. Considering the shift of the spectrum of the cluster of about 0.8 eV with respect to the one of the molecules, these two features may correspond to the high β values associated with the 5a''-3a'' orbitals in the molecular case[57]. This observation confirms the dominant contribution in these two regions of the spectrum of bands built by combination of π-orbitals of the different molecules.

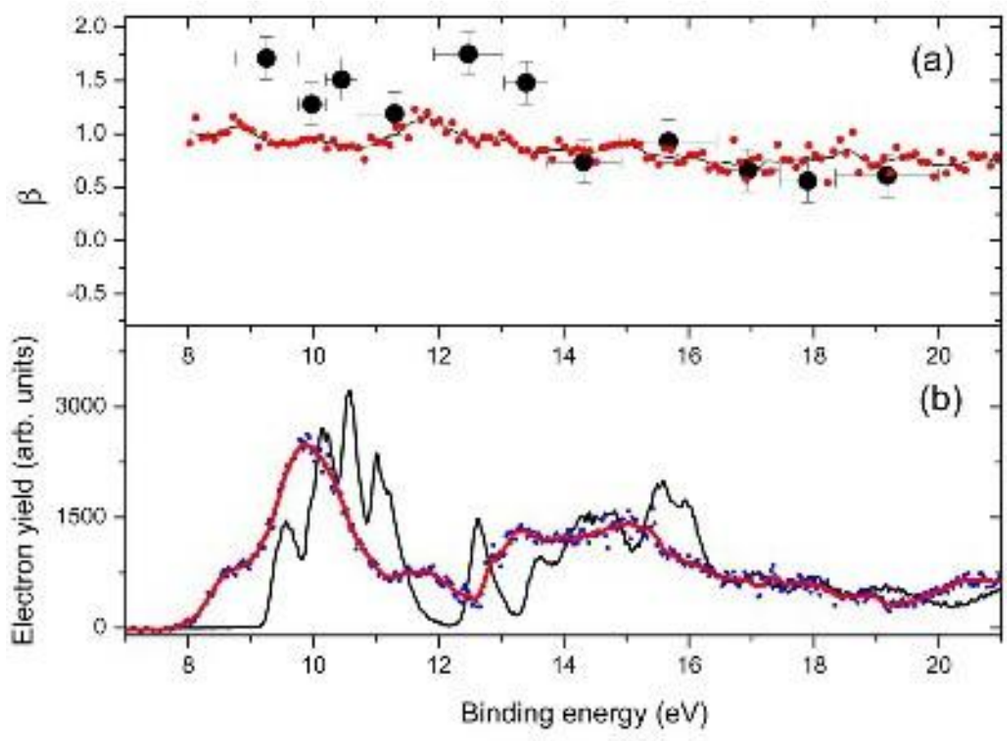

Figure 4: (a) The asymmetry parameter β (red dots) of the uracil clusters measured at 80 eV compared with the β of the molecule (black dots) from ref. [57] measured at 40 eV. (b) The photoelectron spectra of the molecule[24] (black line) and of the uracil clusters (blue dots -experimental values; red curve -smoothed values).

5. Discussion

5.1 Uracil clusters

To simulate the measured spectra a bottom-up approach has been adopted starting from the isolated molecule up to the hexamer in the case of the OVGF and EOM-CCSD methods, and to the dodecamer using DFT. High level OVGF and EOM-CCSD methods have been used as a benchmark for DFT simulations. However, the size of the simulated clusters at the former levels of theory has been limited to six uracil molecules in order to make the calculations affordable. Such a limit can be largely overcome by DFT. Ground state simulations offer in this case a cheap yet sound estimate of the ionization energies of clusters with up to twelve molecules, a sensible upper limit already tested in the case of core-shell photoemission[16]. The ionization energies of all simulated clusters are listed in the

S3 section of Supplementary Information. To compare theoretical predictions with the experiments, Kohn-Sham eigenvalues have been convoluted in a density of states with a Voigt profile with full width at half maximum (FWHM) of 0.7 eV, combining a Gaussian and a Lorentzian function with equal weight and width. This roughly takes into account the experimental energy resolution as well as the vibrational broadening.

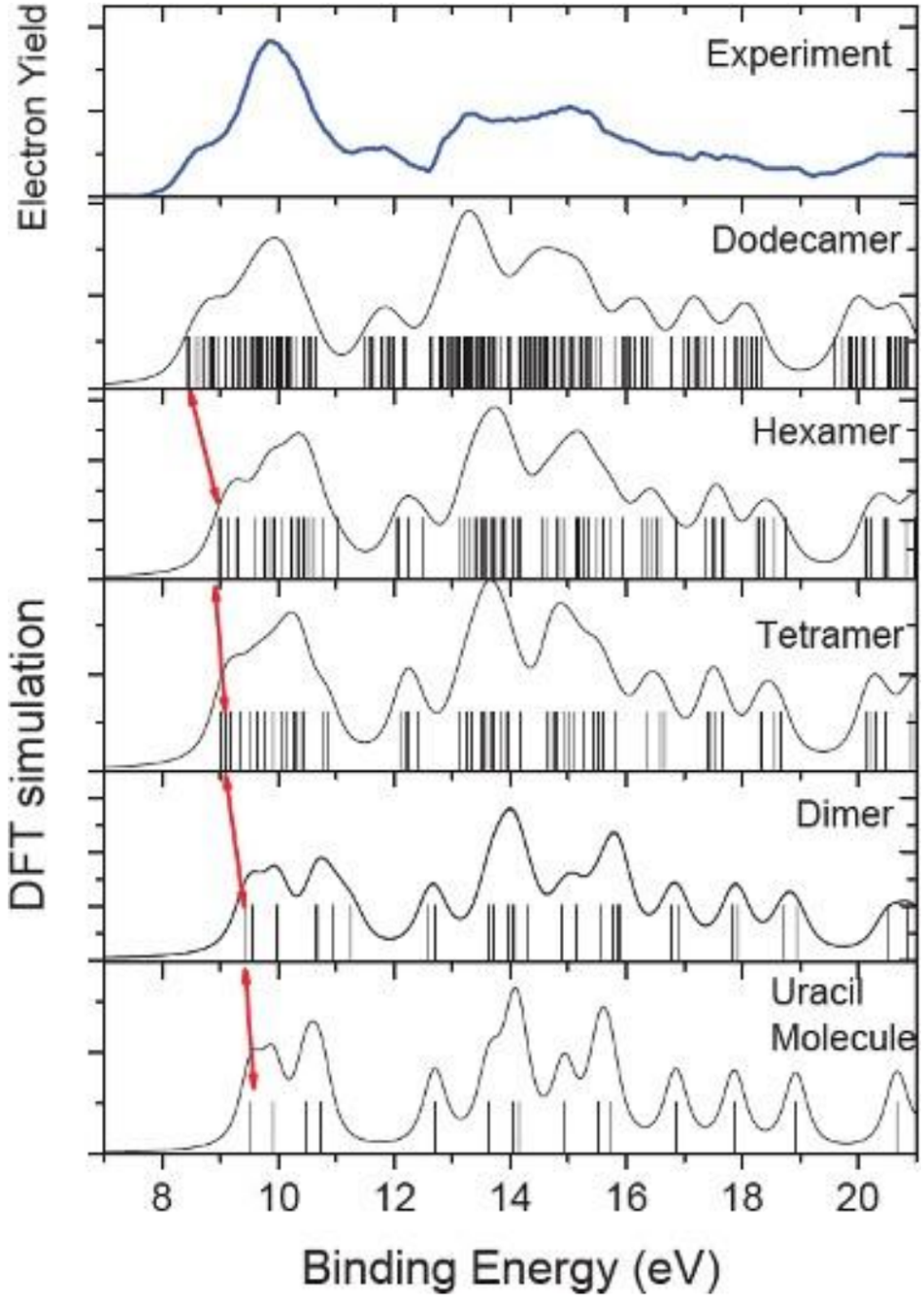

Figure 5: DFT calculated photoelectron spectra of uracil molecule and clusters up to the dodecamer compared with the experimental spectrum of the uracil clusters (top panel). The theoretical density of

states has been convoluted with a Voigt profile (FWHM=0.7 eV) combining a Gaussian and a Lorentzian function with equal weight and width and shifted by 2.3 eV (see text)

In Figure 5 the evolution of DFT-based photoelectron spectra of the uracil clusters of increasing size and its comparison with the experimental spectrum is shown as an example. The calculated spectra have been shifted on the binding energy scale by the same amount needed to match the IP of the isolated molecule with the experimental one (see Table 1). The calculated spectra display a progressive red shift of the ionization potential. As shown in Figure 6, where the difference between the average energy of the states in the outmost band of the cluster spectra and the IP of the uracil molecule calculated with the different methods is reported, the shift tends towards the experimental value.

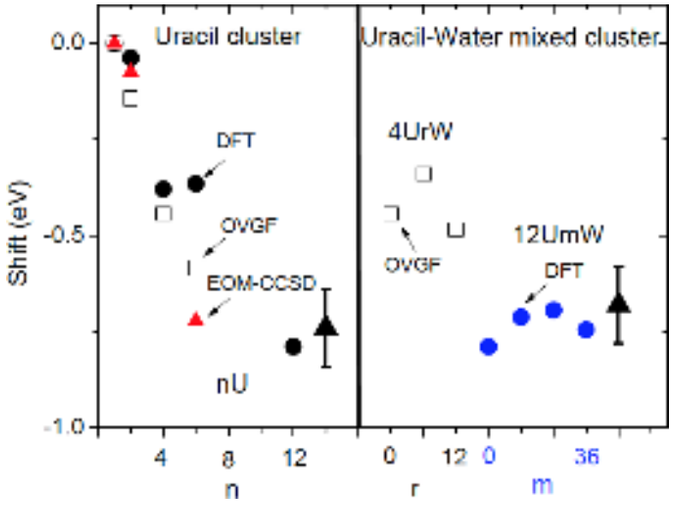

Figure 6: Shift of the average energy of the states in the outmost band of the cluster spectra and the IP of uracil molecule calculated with the OVGF (open square), DFT (dots) and EOM-CCSD (red triangle) methods and measured in the experiment (full black triangle). (left panel) Homogenous uracil clusters nU (n-number of uracil molecules); (right panel) Mixed uracil-water clusters containing 4 and 12 uracil molecules, respectively (r and n- are numbers of water molecules).

The other main features of the spectrum are represented by two broad structures, the former between 9-13 eV and the latter between 13 and 18 eV, separated by a minimum at about 13 eV. Both structures are qualitatively well represented by the calculated spectra. These results indicate that the dodecamer can be already considered as an educated guess of the measured sample.

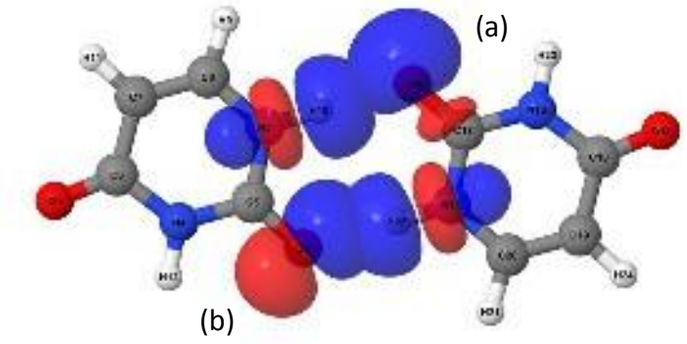

Figure 7: Hydrogen bond interactions in the uracil dimer. The letters (a) and (b) indicate the lone pair (LP(1)), and the lone pair 2 (LP(2)) respectively.

To gain insight in the stabilizing role of H-bonding in uracil clusters, a Natural Bond Orbital (NBO) analysis has been performed on the structures reported in Figure 1, panels (b), (c) and (d). A summary of the selected electron donor and acceptor orbitals, as well as the interaction stabilization energies involved in the H-bonding in the case of the uracil dimer is shown in Table 2. The interaction classification is based on the characteristics of the orbitals of the oxygen lone pairs involved in the hydrogen bond interaction. Adopting the same notation used in the NBO program[37] these orbitals are identified as LP(1) and LP(2). By looking at the plot in Figure 7 it is clear that the LP(1) is very close to an s-type orbital while the LP(2) is a p-type orbital. Such symmetry characteristics are also shared to a greater extent by these lone pairs when water molecules will be considered. The structures are stabilized by N—H···O hydrogen bonds between the carbonyl (C=O) and amide (N-H) groups of the uracil molecules. σ indicates an anti-bonding orbital localized on the N-H bond acting as an acceptor. In the case of a dimer, the E(2) value related to LP(1) on the two oxygen atoms is 10.5 kcal mol^{-1}, while for the LP(2) such a contribution is 20.8 kcal mol^{-1}. These high energies are compatible with a configuration of the structure that results in high orbital overlap between the second lone pair donor orbitals and the anti-bonding orbitals as illustrated in Figure 7.

A similar analysis has been performed for the tetramer and hexamer uracil clusters. The corresponding stabilization energies are reported in Table 7.SI of Supplementary Information.

While in both the tetramer and hexamer the contributions of the LP(1) interactions to the stability are on average similar to those of the dimer, the contributions of the LP(2) interactions are definitely smaller (7.1 and 8.2 kcal mol^{-1}).

Such a behavior is due to the nodal plane in LP(2) (Figure 7b), which makes the E(2) of LP(2) more directionally dependent in comparison to the interactions involving LP(1). Overall, as shown in Figure 1c-d, the uracil molecules in the tetramer and hexamer clusters assume a cage-like structure, rather than the planar configuration of the dimer. In these structures, the LP(2) interactions are not necessarily favored, as is the case in the dimer.

Table 2: Second-order perturbation energies $E(2)$ (kcal mol^{-1}) of the hydrogen bonds in uracil dimers. The numbering of the atom is the same of Figure 7.

Cluster	Donor (i)	Acceptor (j)	$E(2)$	ΔE	$F(i,j)$
Dimer 2U	LP(1)O2	σ*N15—H22	10.50	1.67	0.118
	LP(2)O2	σ*N15—H22	20.80	1.23	0.145
	LP(1)O14	σ*N3—H10	10.52	1.67	0.118
	LP(2)O14	σ*N3—H10	20.86	1.23	0.145

5.2 Mixed water-uracil clusters

In the case of mixed water-uracil clusters, a four-uracil, twelve-water cluster has been chosen as target system for the OVGF calculations, with the primary purpose of performing the same kind of analysis discussed above for uracil clusters. On the other hand, clusters containing twelve uracil molecules and up to thirty-six water molecules, more realistic at the operating conditions of the aggregation source in the present experiment, have been considered by DFT simulations (Figure 8) to provide accurate interpretation and assignment of the measured spectrum, a task impossible without computational support.

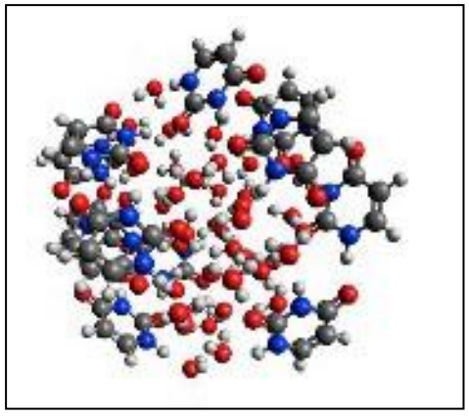

Figure 8: The most stable structures of clusters containing twelve uracil molecules and thirty-six water molecules from Mattioli et al. [17].

Both simulations (see Figure 6) are in agreement with the tiny blue shift of the mixed clusters with respect to the homogeneous ones observed in the experiment, with DFT results better approaching the measured values. Indeed, a cluster with twelve uracil molecules and a few tens of water molecules represents a reasonable first guess of the experimental sample. However, different contributions in the sample must be accounted for to obtain a close similarity between measurements and simulations. Namely, we also expect to find in the spectrum contributions from mixed clusters, pure uracil clusters, pure water clusters and water uncondensed molecules in the experimental beam, as suggested by our previous analysis of the O 1s XPS spectrum of the same mixed clusters[17]. In the panels of Figure 9 the DFT simulated spectrum for a dodecamer uracil cluster, a mixed cluster with twelve uracil and thirty-six water molecules, a cluster with thirty-six water molecules and the photoelectron spectrum of water molecules measured by Truesdale *et al.*[62] are shown. The water photoelectron spectrum of ref. [62] has been chosen among the several present in literature because it displays an energy resolution comparable with the one of the present measurements. The binding energy scale of the DFT simulated spectrum of the cluster with thirty-six water molecules has been established by calculating the difference between the values of the HOMO orbital of the water molecule in the DFT and the EOM-CCSD models and then applying the same shift to the calculated DFT cluster spectrum.

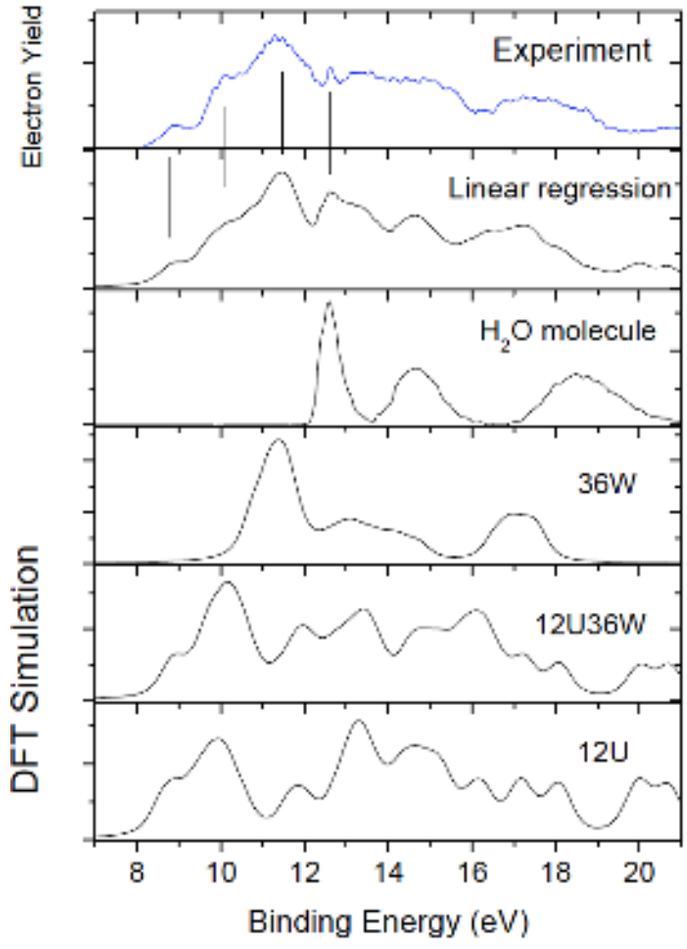

Figure 9: In the panels from bottom to top the simulated DFT spectra of a dodecamer uracil cluster, a mixed cluster with 12 uracil and 36 water molecules, a water cluster with thirty-six molecules, the photoelectron spectrum measured in [62], a linear combination of the four spectra (see text) and the experimental photoelectron spectrum of the mixed water-uracil clusters.

All the simulated spectra have been normalized to the same total area and their combination fitted via a multiple regression to the measured one. Despite the fact that the simulated spectra do not account for the relative cross sections of the different states, a reasonable representation of all the main features of the measured spectrum is achieved with contributions of about 43, 38 and 8% of mixed, pure water and pure uracil clusters and 11% of water molecules. This result is consistent with the predicted structure of mixed clusters, where water forms tightly packed cores and uracil form a shell around these cores. Indeed the water molecules in such cores are responsible for the prominent peak at about 10.2 eV, as shown in S4 Figure 3.SI of Supplementary Information where the 12U36W DOS shown in Figure 9 is projected on water atomic orbitals. On the other hand, the strongest

signal blue-shifted at about 11.3 eV, in the measured spectrum is attributed to the presence of a significant amount of pure water clusters in the best fit of the spectrum.

Table 3: Count of different types of H-bonds and $E(2)_{avg}$ observed in mixed (2U6W, 4U6W and 4U12W)uracil-water clusters.

H-bond type	Donor	Acceptor	Count	E_{avg}(Kcal mol^{-1})
$O_w—H_w\cdots O_u$	$LP(1)O_u$	$\sigma^*O_w—H_w$	20	10.79
	$LP(2)O_u$	$\sigma^*O_w—H_w$	16	9.71
$N_u—H_u\cdots O_w$	$LP(1)O_w$	$\sigma^*N_u—H_u$	0	-
	$LP(2)O_w$	$\sigma^*N_u—H_u$	8	30.56
$O_w—H_w\cdots O_w$	$LP(1)O_w$	$\sigma^*O_w—H_w$	6	8.16
	$LP(2)O_w$	$\sigma^*O_w—H_w$	20	21.34
$N_u—H_u\cdots O_u$	$LP(1)O_u$	$\sigma^*N_u—H_u$	6	9.66
	$LP(2)O_u$	$\sigma^*N_u—H_u$	5	11.71

The NBO analysis of the water-uracil clusters reveals that the mixed structures are stabilized by H-bonds between uracil molecules, water molecules and both uracil and water molecules. Table 3 shows the total count of different types of hydrogen bonds observed in the mixed nUmW cluster. In order to distinguish where these interactions are localized, we add the subscript letters U (uracil) and W (water). According to our calculations, the interactions involving a $\sigma^*O_w—H_w$ orbital, and either an O_w or O_u lone pair are clearly dominant in the stabilization of the mixed clusters, as they represent 76.5 % of all hydrogen bonds under consideration. The electron donor and acceptor orbitals, and the interaction stabilization energy for the clusters with 2 uracil and 6 water molecules, 4 uracil and 6 or 12 water molecules are reported in Table 8.SI of Supplementary Information. The mixed dimer cluster (2U6W) is completely stabilized by water-involving H-bonds. The $N_u—H_u\cdots O_u$ interactions in this clusters have disappeared in favor of interactions with water molecules. In this regime the uracil molecules are stacked[17], making the formations of $N_u—H_u\cdots O_u$ hydrogen bonds impossible.

By comparing the $O_w—H_w\cdots O_u$ and $N_u—H_u\cdots O_w$ interactions in Table 8SI one sees that the orbital LP(2) in the latter bond is the most stabilizing one with an average value of 29.20 kcal mol^{-1}, thus explaining the preferred direct connection of a stacked uracil dimer with water. Similarly, the uracil-uracil H-bonds in the mixed tetramer clusters are limited in favor of water-involving interactions.

Both in $N_u—H_u\cdots O_w$ and $O_w—H_w\cdots O_w$ interactions the LP(2) plays a major role in the stabilization of these clusters. The former contributing on average 35.10 and 28.90 kcal mol^{-1} in the 4U6W and 4U12W cluster respectively, while the latter contributes

approximately 22 kcal mol^{-1} on average in both. These values and the dominance of the interactions involving the water molecules directly with the uracil cluster suggest an interaction mechanism closer to hydration rather than solvation. This is further proven by the relative abundance of the $O_w—H_w\cdots O_u$ hydrogen bond type (Table 3) which involves the C=O bonds of uracil. From Table 3 it is clear how among the 81 interactions considered, 44 involve uracil- water interactions (54%). Among these 36 are $O_w—H_w\cdots O_u$ (82%) and the remaining (18%) are $N_u—H_u\cdots O_w$. The other interactions mainly involve water molecules only (32% of $O_w—H_w\cdots O_w$), with a residual 14% of $N_u—H_u\cdots O_u$ involving uracil molecules only. The relative abundance of the interactions between the uracil C=O moieties and the water molecules, together with the tendency to cohesion among water molecules, suggest a general preference for a mechanism of hydration in the analyzed subset of small clusters, with the attachment of water molecules in a specific position, like in the case of extended hydrated complexes[63,64]. When the same considerations are extended to larger clusters, they lead the assembly of aggregates toward a regime in which the strong cohesion between water molecules through $O_w—H_w\cdots O_w$ bonds favors the formations of water clusters, that can be also found as isolated objects in experimental samples. In this regime, where $O_w—H_w\cdots O_u$ connections can pin the uracil shell to the water core and $N_u—H_u\cdots O_u$ connections maintaining a residual connectivity across the uracil shell.

As a further evidence of the mentioned above effects and their specificity, the strong interactions between the uracil clusters and the surrounding water molecules are readily visible in the bond length variations in the uracil molecules. To this aim we considered the clusters with 4 uracil molecules with respect to an increasing number of water molecules. Table 6.SI in S6 of Supplementary Information shows the bond lengths for each of the four uracil molecules in the 4UnW (n=0,6,12) clusters. The double C=O bond elongates as the number of water molecules *n* increases as shown in Figure 10. The average C=O bond length versus the number of water molecules *n* is well represented by a linear relation

$$R = 0.0041n + 1.2259$$

with a correlation coefficient $r^2 = 0.912$. The N—H and C—H bonds remain fairly constant, with some variations likely due to an incidentally strong interaction due to the irregular cluster arrangement.

Finally an attempt has been made to relate the results of the OVGF calculations with the E(2) energies from NBO calculations. Both the values derived from the intermolecular interactions and total values have been considered for the E(2) results. A linear correlation has been found with the total value obtained from the difference between OVGF and Koopmans Theorem, KT, results related to the orbitals under the peaks of the simulated photoelectron spectra at the OVGF/6-31G level (Fig. 4a.SI in S5 Supplementary Information) and the computed E(2), which holds for both the total and the hydrogen bond related results. Such a correlation finds its rationale if we consider that both the OVGF results[65,66] and the E(2) are obtained through perturbative approaches. Figure 11 shows the results. The analysis is limited to the first peak of the photoelectron spectra, which reasonably includes the most significant molecular orbitals responsible for the interactions between the molecules and is well separated in all spectra. The correlation found, suggests that the OVGF corrections of the ionization energies provide a picture of the stabilization energy within molecular clusters of increasing size through a simple extrapolation model based upon NBO analysis.

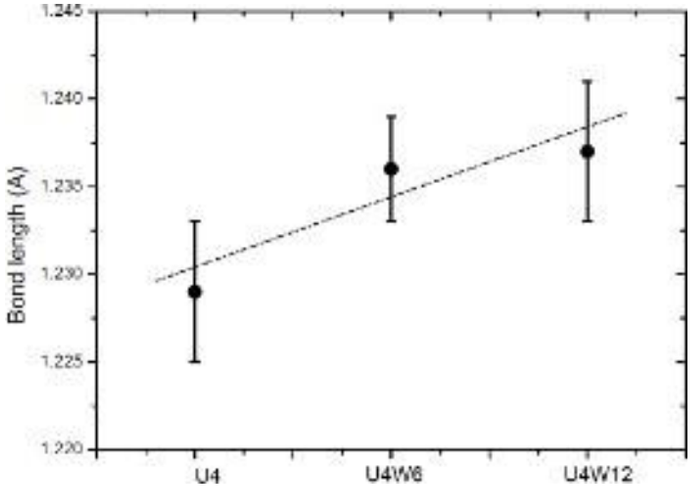

Figure 10*:* Linear fit of the variations of the C=O average bond length against the tetramer mixed cluster size.

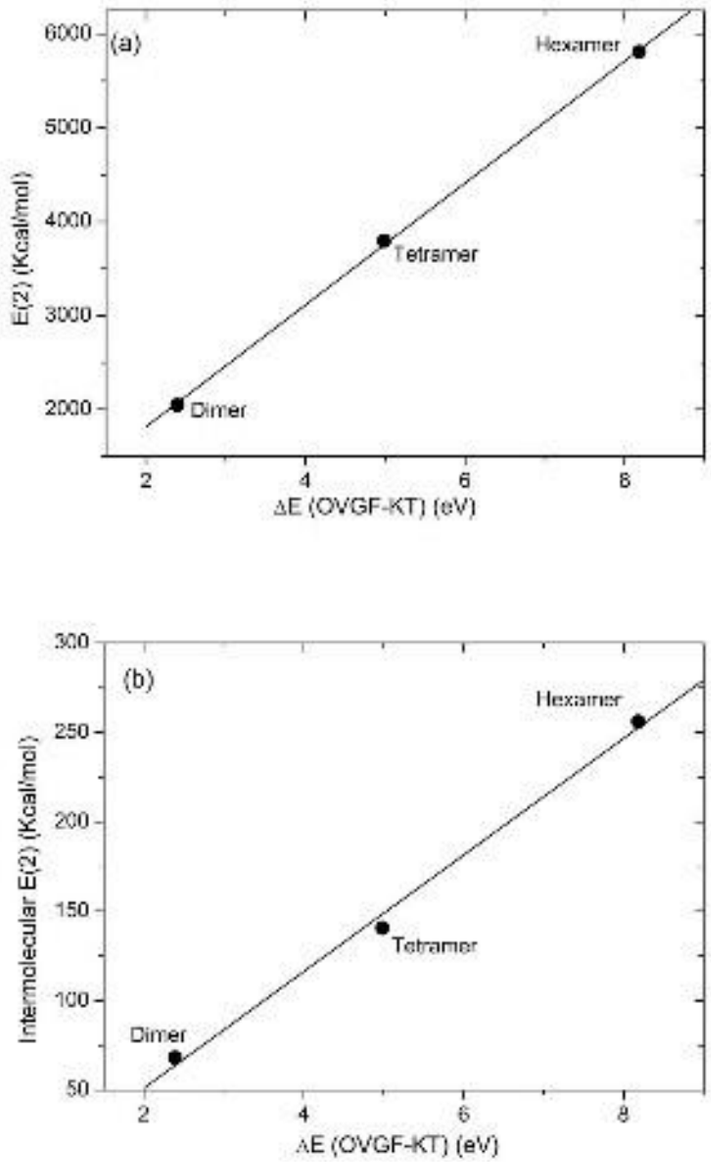

Figure 11: Correlation between the E(2) and the total ΔE (OVGF-KT) for the first peak of the OVGF simulated spectra. In (a) the total E(2) and in (b) only the intermolecular contribution to E(2) are shown.

6 Summary and Conclusions

The valence photoelectron spectra of uracil and mixed water-uracil clusters produced by a gas aggregation source have been measured with synchrotron radiation.

The main observation in the experimental spectra, i. e. the red shift of the IP, the number and broadening of the features in the spectra and the rise of a broad feature centered at about 11.3 eV in the case of the mixed water-uracil clusters, have been correctly represented by the theoretical simulations of the spectra.

The red shift is interpreted as an extended conjugation among molecules through the H bond between CO and NH moieties. Unexpectedly, there are distinct features related to water aggregation. The structure at about 11.3 eV in mixed clusters is assigned to pure

water clusters, resolved from both contributions of water cores enclosed within uracil shells (broad feature peaked at about 10.2 eV), and from the sharp feature at about 12.6 eV assigned to uncondensed water molecules. The latter observations confirm therefore the core-shell structure[17] predicted for the mixed clusters, where the tightly-packed network of the water molecules forms an inner core with the uracil molecules pinned as an external shell.

The same spectra have been also simulated using a bottom-up approach to identify cluster structures, previously assessed on XPS spectra[16], and to validate them against the experiment. The novelty of the present work is also represented by the fact that the simulation of the valence spectrum provides the opportunity of an accurate and quantitative comparison between low-level and high-level methods. In particular, this has been done through an inner comparison between expensive and accurate wavefunction-based methods (e.g., OVGF and EOM-CCSD) and much more affordable DFT-based estimates, applicable to large clusters.

The obtained results show that a reasonable theoretical representation of the valence photoionization spectrum is obtained with clusters of small size, made by a dozen of uracil molecules and some tens of water molecules.

The satisfactorily reproduction of the main features of the experimental spectra, confirm the validity of the structures predicted by the semiempirical tight-binding method and, more generally, the validity of our multi-level approach to the investigation of complex non-covalent structures in gas-phase.

A NBO analysis then enriches the description of the H-bond connectivity of pure and mixed clusters by providing accurate quantitative estimates of the stabilization energy corresponding to the formation of strong hydrogen bonds. In mixed clusters containing water molecules, favored donor-acceptor pairs show a tendency to form at specific positions, generally favoring the H-O-H...O=C connectivity and the water cohesion, as also indicated by a selective elongation of the C=O bond and by the correlation between stabilization energies and ionization energies in smaller clusters. This gives a quantitative information on the reasons that induce the formation of a wide range of clusters in the mixed-molecule regime, dominated by the presence of water cores that occur as “stripped” (38% of the sample) or “dressed” by uracil shells (43% of the sample), due to the interplay between different values of the calculated second-order perturbative energies E(2).

Supplementary Material

See supplementary material for the calculated spectra of the uracil molecule and the uracil dimer with different basis sets, the tables of the occupied electronic states of uracil and mixed water-uracil clusters, the tables of second-order perturbation energies and a comparison of the density of states of pure uracil cluster (12 uracil molecules), mixed uracil-water cluster (12 uracil and 36 water molecules) and pure water cluster (36 water molecules) systems calculated using three different exchange-correlation functionals

Acknowledgments

This article is based upon work from COST Action CA18212 - Molecular Dynamics in the GAS phase (MD-GAS), supported by COST (European Cooperation in Science and Technology) and it has been partially supported by CNRS PICS Project BIFACE, and International Associated Laboratory "DYNAMO", the PRIN 20173B72NB “Predicting and controlling the fate of bio-molecules driven by extreme-ultraviolet radiation”. C.N. is co-funded by Région Normandie and Synchrotron SOLEIL. SOLEIL support is acknowledged under project no. 20171346. AC acknowledges the access to the CINECA supercomputer facility via the ISCRA C HP10C652JX grant. F.M. and T.V.C. acknowledge the VSC (Flemish Supercomputer Center), funded by the Research Foundation-Flanders (FWO) and the Flemish Government.

DATA AVAILABILITY

The data that support the findings of this study are available from the corresponding author.

Reference

[1] Prince, K.C.; Bolognesi, P.; Feyer, V.; Plekan, O.; Avaldi, L. *J. Electron Spectrosc. Rel. Phenom.* **2015**, *204*, 335.

[2] Robertson, E. G.; Simons, J. P. *Phys. Chem. Chem. Phys.* **2001**, *3*, 1–18,

[3] Tomoda, S.; Achiba, Y.; Kimura, K. *Chem. Phys. Lett.* **1982**, *87*,197-200

[4] Öhrwall, G.; Fink, R.F.; Tchaplyguire, M; Ojamäe, L.; Lundwall,M.; Marinho, R.R.T.; Naves de Brito, A.; Sorensen, S.L.; Gisselbrecht, M.; Feifel, R.; Rander, T.; Lindblad, A.; Schulz.,J.; Sæthre, L.J.; Mårtensson, N.; Svensson, S.; Björneholm, O. *J.Chem. Phys.* **2005**,*123*, 054310.

[5] Björneholm, O.; Federmann, F.; Kakar,S.; Moller, T *J.Chem. Phys.* **1999**, *111*, 546.

[6] Barth, S.; Oncak, M.; Ulrich, V.; Mucke, M.; Lischke, T.; Slavicek, P.; Hergenhahn, U. J. *Phys. Chem. A* **2009**, *113*, 13519.

[7] Schlatholter, T.; Alvarado, F.; Bari, S.; Lecointre, A.; Hoekstra, R.; Bernigaud, V.; Manil, B.; Rangama, J.; Huber, B. *ChemPhysChem* **2006**, *7*, 2339.

[8] Markush, P.; Bolognesi, P.; Cartoni, A.; Rousseau, P.; Maclot, S.; Delaunay, R.; Domaracka, A.; Kočišek, J.; Castrovilli, M. C.; Huber, B. A.; Avaldi, L. *Phys.Chem.Chem.Phys.* **2016**, 18, 16721.

[9] Castrovilli, M. C.; Markush, P.; Bolognesi, P.; Rousseau, P.; Maclot, S.; Cartoni, A.; Delaunay, R.; Domaracka, A.; Kocisek, J.; Huber, B. A.; Avaldi, L. *Phys.Chem.Chem.Phys.* **2017**, *19*, 19807.

[10] Domaracka, A.; Capron, M.; Maclot, S. ; Chesnel, J.Y.; Méry, A.; Poully, J.C.; Rangama, J.; Adoui, L.; Rousseau, P.; Huber, B.A. *J. Phys.: Conf. Ser.* **2012**, *373*, 012005
[11] R Maisonny, R.; Capron,M.; Maclot, S.; Poully, J. C.; Domaracka, A.; Méry, A.; Adoui, L.; Rousseau, P.; Huber, B. A. *J. Phys.: Conf. Ser.* **2013**, *438* 012007
[12] Barc, B.; Ryszka, M.; Spurrell, J.; Dampc, M.; Limão-Vieira, P.; Parajuli, R.; Mason, N. J.; Eden, S. *J. Chem. Phys.* **2013**, *139*, 244311.
[13] Kim, N.J.; Kang, H.; Jeong, G.; Kim, Y.S.; Lee, K.T.; Kim, S.K. ***J***. *Phys. Chem. A* **2000,** *104*, 6552
[14] Kočišek, J.; Pysanenko, A.; Farnik, M.; Fedor, J. *J. Phys. Chem. Lett.* **2016**, *7*, 3401.
[15] Poštulka, J.; Slavíček, P.; Fedor, J.; Fárník, M.; Kočišek J. *J. Phys. Chem. B* **2017**, *121*, 8965.
[16] Mattioli, G.; Avaldi, L.; Bolognesi,P.; Bozek, J. D.; Castrovilli, M. C.; Chiarinelli, J.; Domaracka, A.; Indrajith, S.; Maclot, S.; Milosavljević, A. R.; Nicolafrancesco, C.; Nicolas, C.; Rousseau, P. *Sci. Rep.* **2020**, *10*, 13081.
[17] Mattioli, G.; Avaldi, L.; Bolognesi,P.; Bozek, J. D., Castrovilli, M. C.; Chiarinelli, J.; Domaracka, A.; Indrajith, S.; Maclot, S.; Milosavljević, A. R.; Nicolafrancesco, C.; Nicolas, C.; Rousseau, P *Phys.Chem.Chem.Phys.* **2021**, 23, 1859.
[18] Cederbaum, L. S.; Domcke, W. *Adv. Chem. Phys.* **1977**, *36*, 205.
[19] von Niessen W.; Schirmer J.; Cederbaum L. S. *Comput. Phys. Rep.* **1984**, *1*, 57.
[20] Molteni, E. ; Mattioli, G.; Alippi, P.; Avaldi, L. ; Bolognesi, P.; Carlini, L. ; Vismarra, F.; Wu, Yingxuan; Borrego Varillas, R. ; Nisoli, M.; Singh, M. ; Valadan, M.; Altucci, C.; Richter R.; Sangalli D. *Phys.Chem.Chem.Phys.* **2021**, *23*, 26793.
[21] Stanton, J. F.; Bartlett, R. J. *J. Chem. Phys.* **1993**, *98*, 7029.
[22] Lindblad, A.; Söderström, J.; Nicolas, C.; Robert, E.; Miron, C. *Rev. Sci. Instrum.* **2013**, *84*, 113105.
[23] Nicolafrancesco, C.; Hartweg, S.; Gil, J.-F.; Robert, E.; Ramillon, J.M.; Nicolas, C.; Indrajith, S.; Bozek, J. D.; Nahon, L.; Milosavljević, A.R.; Rousseau, P. *E. Phys. J. D* **2021**, *75*, 117.
[24] Feyer, V. et al. *private communication* **2009.**
[25] Plekan, O.; Feyer, V.; Richter, R; Coreno, M.; de Simone, M.; Prince, K.C.; Trofimov, A.B.; Gromov, E.V.; Zaytseva, I.L.; Schirmer, J. *J. Chem. Phys.* **208**, *347*, 360.
[26] Bannwarth, C.; Ehlert, S.; Grimme, S. *J. Chem. Theory Comput.* **2019**, *15*, 1652.
[27] Grimme, S. *J. Chem. Theory Comput.* **2019**, *15*, 2847.
[28] Pracht, P.; Bohle, F.; Grimme, S. *Phys.Chem.Chem.Phys.* **2020**, *22*, 7169
[29] Giannozzi, P.; Andreussi, O.; Brumme, T.; Bunau, O.; Nardelli, M. B.; Calandra, M.; Car, R.; Cavazzoni, C.; Ceresoli D., et al. *Phys. Condens. Matter* **2017**, *29*, 465901.
[30] Giannozzi, P.; Baroni, S.; Bonini, N.; Calandra, M.; Car, R.; Cavazzoni, C.; Ceresoli, D.; Chiarotti, G. L.; Cococcioni, M.; Dabo, I.; et al., *J. Phys.: Condens. Matter* **2009**, *21*, 395502.
[31] Neese, F.; *Wiley Interdiscip. Rev.: Comput. Mol. Sci.* **2012**, 2, 73.
[32] Hehre, W. J.; Ditchfield, R.; Pople, J. A. *J. Chem. Phys*. **1972**, *56*, 2257.
[33] Frisch, M. J. et al. Gaussian 09, Revision B.01 Gaussian, Inc., Wallingford CT, **2009**.
[34] Schirmer, J. *Phys. Rev. A* **1982**, *26*, 2395.
[35] Schirmer, J.; Mertins, F. *Int. J. Quantum Chem.* **1996**, *58*, 329.
[36] Trofimov, A. B.; Stelter, G.; Schirmer, J. *J. Chem. Phys.* **1999**, *111*, 9982.
[37] Nakatsuji, H. Chem. *Phys. Lett.* **1979**, *67*, 334.
[38] Nakatsuji, H. Chem. *Phys. Lett.* **1979**, *67*,329.
[39] Deleuze, M.S. *J. Chem. Phys.* **2002**, *116*, 7012; *J. Phys. Chem.* A **2004**, *42*, 9244; *Chem. Phys.* **2006**, *329*, 22
[40] Kendall, R. A.; Dunning, T. H.; Harrisson, R. J. *J. Chem. Phys.* **1992**, *96*, 6796.
[41] Schaefer, A.; Horn, H.; Ahlrichs, R. *J. Chem. Phys.* **1992**, *97*, 2571.
[42] Weigend, F.; Ahlrichs, R. *Phys. Chem. Chem. Phys.* **2005**, *7*, 3297.
[43] Foster, J.P.; Weinhold, F. *J. Am. Chem. Soc.* **1980**, *102*, 7211.
[44] Weinhold, F.; Landis, C.R. *Chemistry Education Research and Practice*, **2001**, *2*, 91.
[45] Sharma, P.; Mitra, A.; Sharma, S.; Singh, H.; Bhattacharyya, D. *J Biomol. Struct. Dyn*. **2008**, *25*, 709.
[46] Ebrahimi, A.A.; Khorassani, S.M.; Delarami, H. *Chem. Phys*. **2009**, *365*, 18.
[47] Reed, A. E.; Carpenter, J. E.; Glendening, E. D.; Weinhold, F. NBO, Version 3.1; Gaussian, Inc.: Wallingford, CT **2009**.
[48] Halder, A.; Data, D.; Seelam, P. P.; Bhattacharyya, D.; Mitra, A. *ACS Omega* **2019**, *4*, 7354.

[49] Lauer, G.; Schäfer W.; Schweigh, A. *Tetrahedron Lett.* **1975**, *16* ,3939.
[50] Dougherty, D.; Wittel, K.; Meeks, J.; McGlynn, S.P. *J. Am. Chem. Soc.* **1976,** *98*, 3815.
[51] Lin, J.; Yu, C.; Peng, S.; Akiyama, J.; Li, K.; Lee, L.-K.; le Breton, P.R. *J. Am. Chem. Soc.* **1980**, *102*, 4627.
[52] Padva, A.; Le Breton, P.R.; Dinerstein, R.J.; Ridyard, J.N.A. *Biochem. Biophys. Res. Commun.* **1974**, *60* ,1262.
[53] Padva, A.; Peng, S.; Lin, J.; Shahbaz, M.; Breton, P.R. *Biopolymers* **1978**, *17*, 1523.
[54] Palmer, M.H.; Simpson, I.; Platenkamp, R. J. *J. Mol. Struct.* **1980,** *66,* 243.
[55] Yu, C.; O'Donnell, T.J.; Breton P.R. *J. Phys. Chem.* **1981**, *85* ,3851.
[56] Kubota, M.; Kobayashi, T. *J. Electron Spectrosc. Relat. Phenom.* **1996**, *82*, 61.
[57] Holland, D.M.P.; Potts, A.W.; Karlsson,L; Zytseva, I.L.; Trofimov,A.B.; Schirmer, J. *Chem. Phys.* **2008**, *353*, 47.
[58] Fulfer, K.D.; Hardy, D.; Aguilar A.A.; Poliakoff E.D. J. *Chem. Phys.* **2015**, *142*, 224310.
[59] Kimura, K.; Katsumata, S.; Achiba, Y.; Yamazaki, T.; Iwata, S*. Hanbook of HeI Photoelectron Spectra of Fundamental Organic Molecules* **1981**, John Wiley & Sons Inc.
[60] Piancastelli, M.N.; Keller,P.R.; Taylor, J.W.; Grimm,F.A.; Carlson,T. A. *J. Am. Chem. Soc.* **1983**, *105*, 4235.
[61] Holland, D.M.P.; Karlsson, L.; von Niessen, W. *J. Electron Spectrosc. Relat. Phenom.* **2001**, *113*, 221.
[62] Truesdale, C.M.; Soutworth, S.; Kobrin, P.H.; Lindle, D.W.; Shirley, D. *J. Chem. Phys.* **1982**, *76*, 860.
[63] Oostenrijk, B.; Barreiro, D.; Walsh, N.; Sankari, A.; Månsson, E. P.; Maclot, S.; Sorensen, S. L.; Diaz-Tendero, S.; Gisselbrecht, M. *Phys. Chem. Chem. Phys.* **2019**, *21*, 25749.
[64] Bacchus-Montabonela, M.-C.; Calvo, F.; *Phys. Chem. Chem. Phys.* **2015**, *17*, 9629.
[65] Ortiz, J. V. *Int. J. Quantum Chem.* **2005**, *105*, 803.
[66] Ortiz, J. V. *WIREs Comput. Mol. Sci.* **2013**, *3*, 123